CHAPTER 6

RESULTS

LITHIUM NICKEL MANAGANESE VANADATE BY THE SOL-GEL METHOD

6.1 Introduction

The interest of improving the performance of the high potential cell of $LiNiVO_4$ has become the most important goal among researchers for the cathode system study. Thus, a number of materials were proposed to become the possible doping source in their cathode systems [Fey and Wu, 1997; Julien *et. al*, 1999; Arrabito *et. al*, 2001; Lai *et. al*, 2002b; Vivekanandhan *et. al*, 2005; Fey *et. al*, 2006; Fey *et. al*, 2007; Thongtem *et. al*, 2008]. Almost all reported works has improved performance in the capacity. However, the reversibility whereby the cell had abrupt decay in capacity upon few cycling has always become the major concern.

In this work, the manganese acetate tetrahydrate was chosen as the doping material in the pristine lithium nickel vanadate. The $LiNi_{1-x}Mn_xVO_4$ ($0 \leq x \leq 1$) was synthesized using the sol- gel (SG) route. The obtained precursor was sintered in various temperatures in the furnace for 3 hours respectively. Subsequently, the treated samples

were characterized by the TGA, XRD, SEM, TEM, EDAX, and cyclic voltammetry (CV).

6.2 Structural studies

6.2.1 X- ray diffraction (XRD)

The second system discuss about the effect of doping material to $LiNiVO_4$ prepared by the sol-gel method. Manganese was used as the doping material to the $LiNiVO_4$. The manganese partial substitution in the octahedral sites by another transition metal may affect the structure as well as the electrochemical properties. X - ray diffraction analyses shown below were carried out to determine the phases and the crystal structure of the sintered product. The reaction for $LiNi_{1-x}Mn_xVO_4$ ($0 \leq x \leq 1$) were also calcined at 500 °C, 600 °C, 700 °C and 800 °C for 3 hours separately and those treatments are stated in Table 6.1.

Table 6.1: Treatment conditions for preparation of $LiNi_{1-x}Mn_xVO_4$ ($0 \leq x \leq 1$)

$LiNi_{1-x}Mn_xVO_4$	Ratio Ni:Mn
V1	0.25:0.75
V2	0.50:0.50
V3	0.75:0.25
V4	0.00:1.00

The crystallographic XRD pattern of $LiNi_{1-x}Mn_xVO_4$ ($0 \leq x \leq 1$) were presented above for $LiNi_{0.25}Mn_{0.75}VO_4$ (V1) , $LiNi_{0.5}Mn_{0.5}VO_4$ (V2), $LiNi_{0.75}Mn_{0.25}VO_4$ (V3), $LiMnVO_4$ (V4) in Figure 6.1, Figure 6.2, Figure 6.3 and Figure 6.4 respectively. The V4 compound which Ni was not added in the synthesis behaves in mixed phase of

$LiMnVO_4$ obtained from 500 °C to 700 °C. The sample for 800 °C cannot be taken out due to hard adherence to the sintering container. The similar phase of $LiNiVO_4$ is expected for the mixed doped system because the substituted material does not change the spinel structure of $LiNiVO_4$ [Lai *et. al*, 2002b].

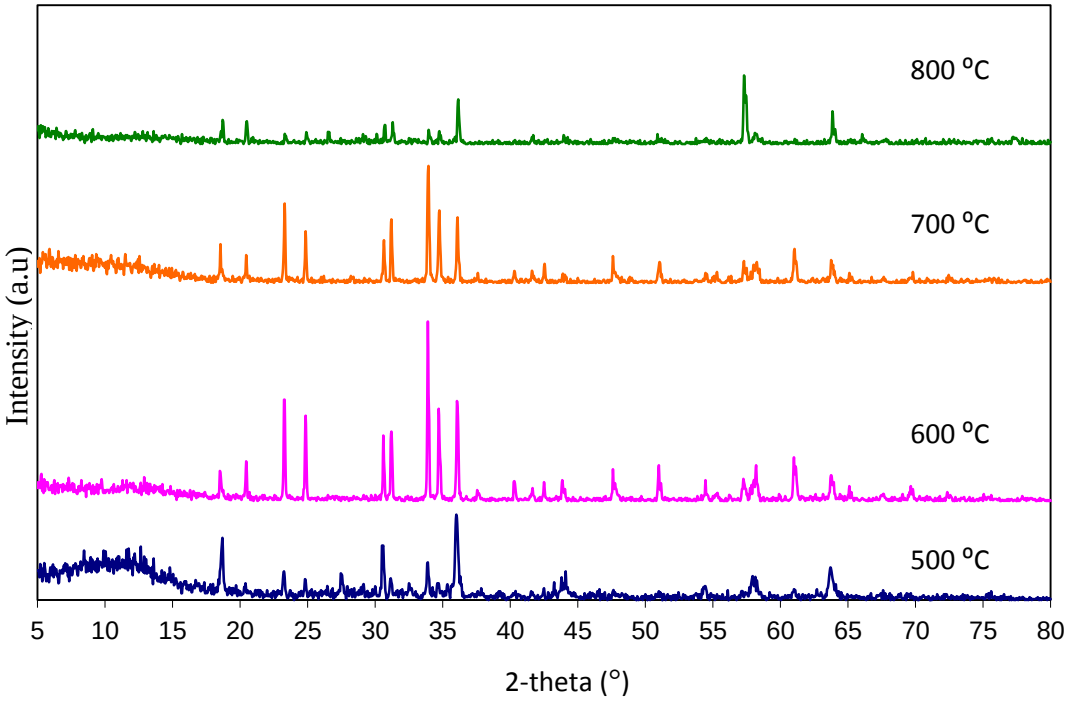

Figure 6.1: XRD pattern for V1 system

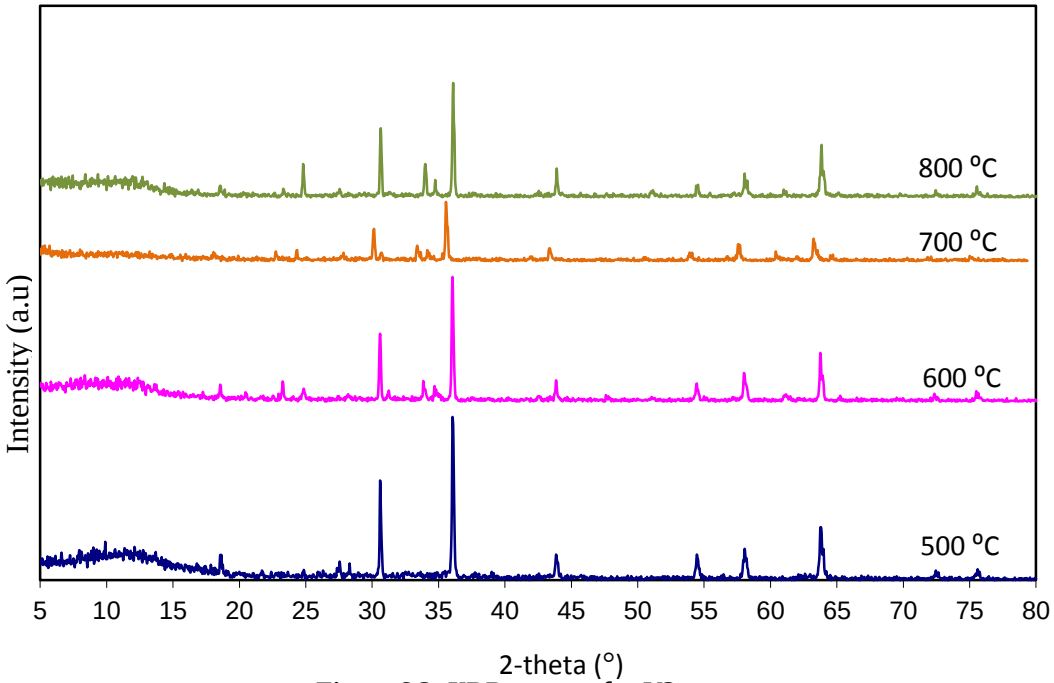

Figure 6.2: XRD pattern for V2 system

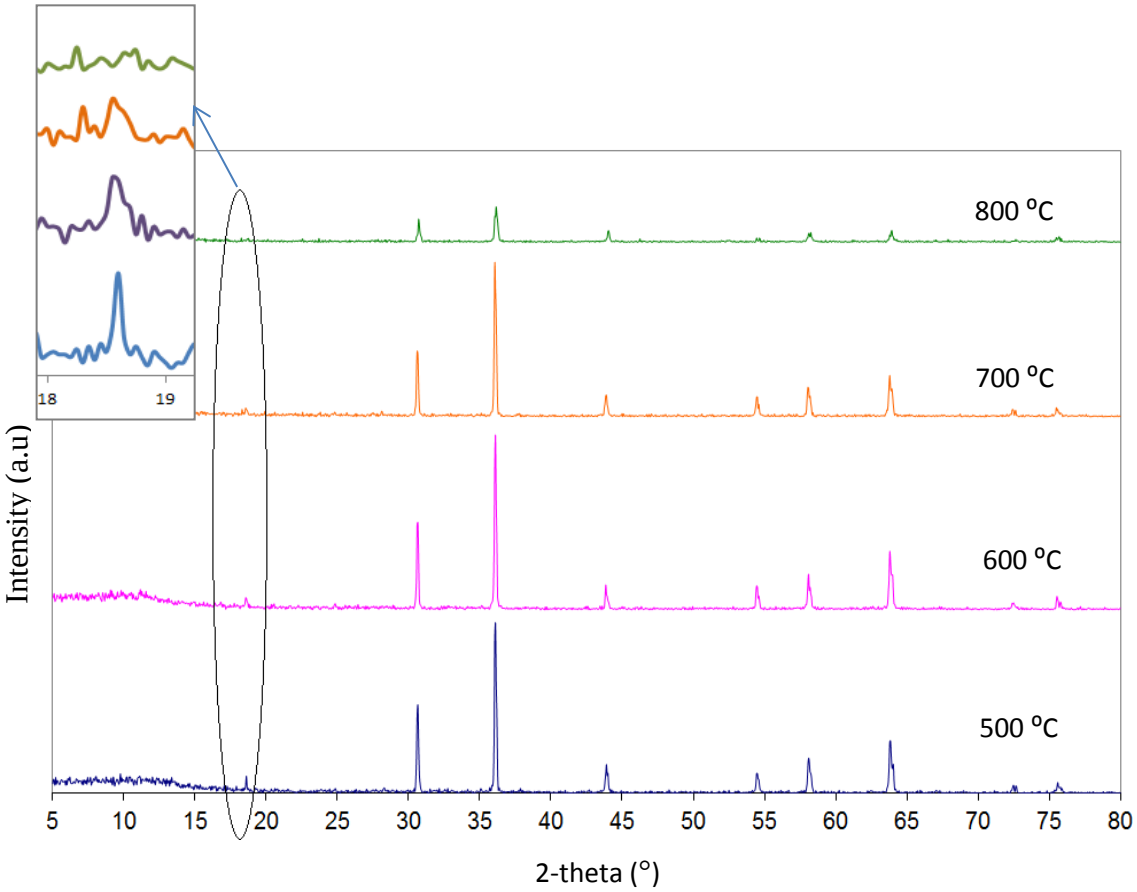

Figure 6.3: XRD pattern for V3 system

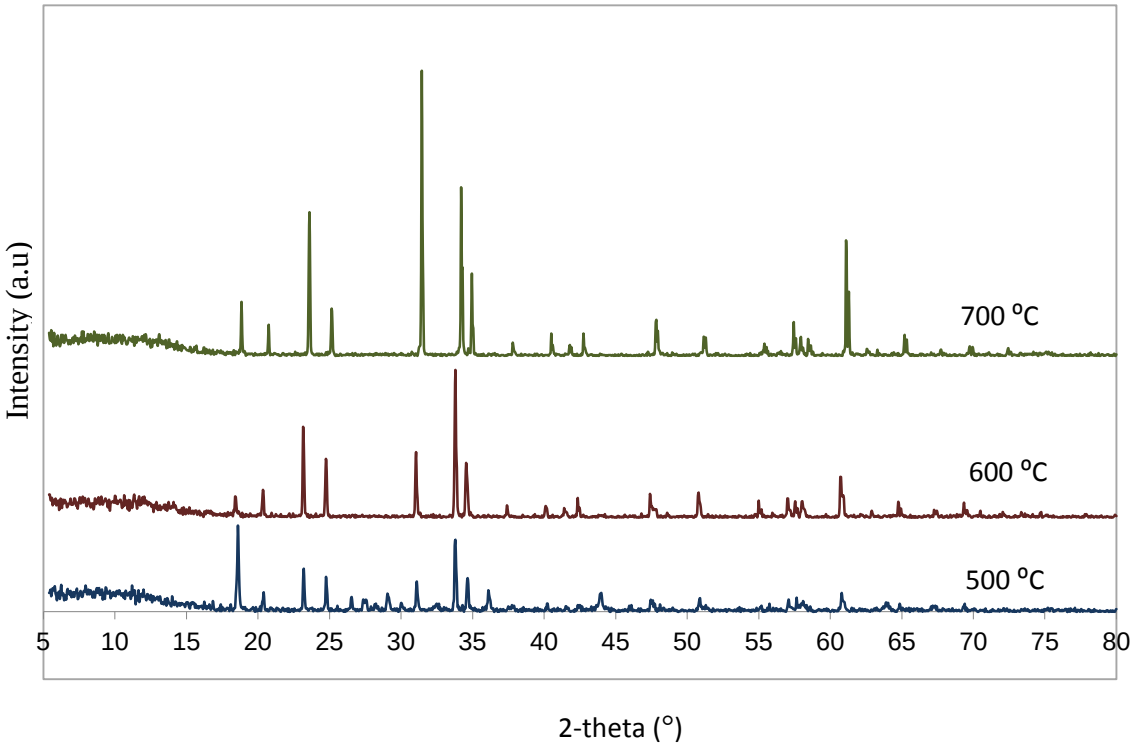

Figure 6.4: XRD pattern for V4 system

According to the XRD patterns presented, all system except the V3 system exhibit the mixed phase of the $LiNiVO_4$. The XRD lines of mixed phase $LiNiVO_4$ in V1, V2 reduces as the ratio of Mn decreases and subsequently lead to the formation of single phase of $LiNiVO_4$ (V3). The V3 sample present in sharp peaks at 2θ = 36.2°, 30.6°, and [111] peak at 18.6°, indicating the sample did crystallize well in the compound. The V3 system is the only system in the mixed doped prepared by sol-gel method that shows the single phase inverse spinel $LiNiVO_4$ compound. The result obtained follows the literature from Lai et. al, (2002b) mentioned that the amounts of replacing nickel by manganese are limited. Their work reports on a tolerable range is of $0 \leq x \leq 0.4$ in the $LiNi_{1-x}Mn_xVO_4$ in which they have reported the compound present at x = 0.4 treated at first sintered for 4 h, then at the same temperature for 3 or 4 h after being ground [Lai *et. al,* 2002b]. The high crystallinity nature of inverse spinel $LiNi_{0.75}Mn_{0.25}VO_4$ by sol-gel method was observed at sample treated at 500 °C, 600 °C, 700 °C, 800 °C, where the calculated intensity ratio of $I_{[220]}/ I_{[311]}$ is 0.52, 0.50, 0.43 and 0.65, respectively.

6.2.2 Crystallite size

Based on the XRD pattern obtained, the corresponding values were taken to calculate the crystallite size of the $LiNi_{1-x}Mn_xVO_4$ ($0 \leq x \leq 1$) system. The Scherrer equation again was used to obtain the crystallite size values. According to the XRD peaks, the sample chosen was V3 system because the composition follows the expected inverse spinel pattern for the XRD diffractogram. The XRD crystallinity for the sample calcined from 500 °C to 600 °C increases based on the sharp peak at both sintering temperature. This result indicates that the sharper increasing peak correspond to the larger particle size at elevated temperature [Chaliha *et. al,* 2008]. Subsequently, the crystalline peak reduces

gradually upon higher sintering temperature at 700 °C and 800 °C. We can expect that the particle size will decrease as such phenomenon depicts in the XRD results. The V3 crystallite size values are shown in Table 6.2. The crystal size between 23 nm- 35 nm was obtained in the calculation in Scherrer equation.

Table 6.2: Crystallite size values for the $LiNi_{0.75}Mn_{0.25}VO_4$ – SG system

Temperature (ºC)	Crystallite Size (nm)
500	33.54
600	35.71
700	32.67
800	23.65

6.2.3 Lattice constants and the volumes of crystal cell

For cubic crystal structure, the lattice parameter, *a* can be calculated by the powder XRD data available in the analysis. The lattice constant can be obtained by using the Braggs formula mentioned in equation (3.3):

$$a = d\left(h^2 + k^2 + l^2\right)^{1/2}$$

Here, *d* is the distance between vicinal crystal face and *hkl* is the Miller index. The data was chosen at the most intense [311] peak. The lattice constants with respective

compound of each system based on the obtained 2- theta value of the [h k l] values are tabulated in Table 6.3.

Table 6.3: Lattice constant value for doped $LiNi_{1-x}Mn_xVO_4$ -SG ($0 \leq x \leq 1$) system

System	2θ (°)	θ(°)	*d* obs.	*a*(Å)
$LiNi_{1.00}Mn_{0.00}VO_4$	36.150	18.075	2.4817	8.231
$LiNi_{0.25}Mn_{0.75}VO_4$	36.000	18.000	2.4917	8.264
$LiNi_{0.5}Mn_{0.5}VO_4$	36.050	18.025	2.4884	8.253
$LiNi_{0.75}Mn_{0.25}VO_4$	36.100	18.050	2.4850	8.242

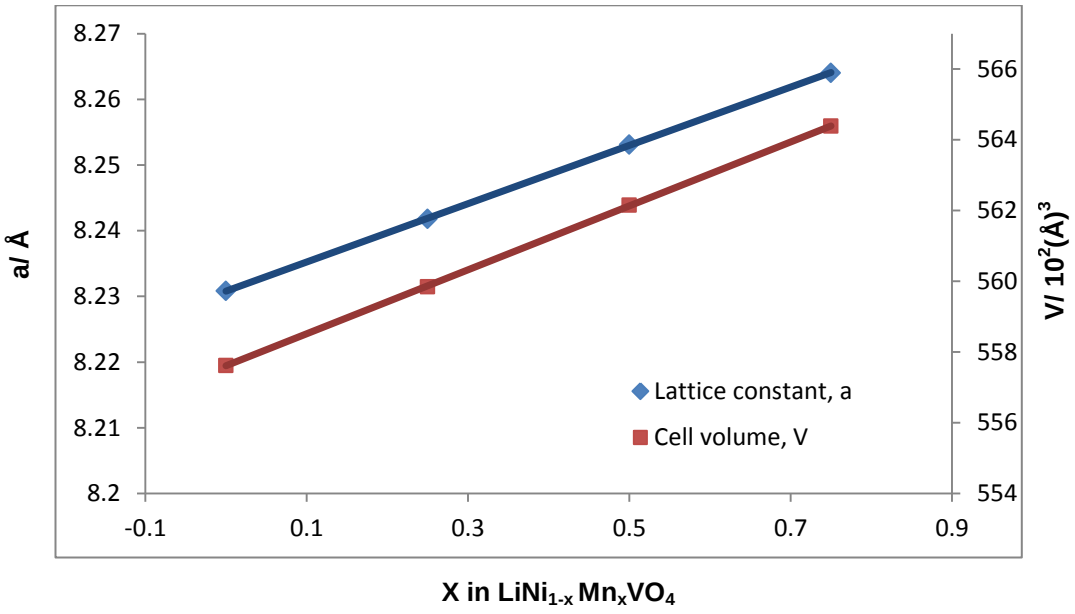

Figure 6.5: Lattice constant, *a* and cell volume, *V* for $LiNi_{1-x}Mn_xVO_4$-SG system ($0 \leq x \leq 1$) at 600 °C

The lattice constant, *a* and cell volume, *V* are plotted in Figure 6.5 for the $LiNi_{1-x}Mn_xVO_4$ by sol-gel method. The relationship of lattice constant, *a* and cell volume, *V* with the manganese content, *x* for the mixed- doped $LiNi_{1-x}Mn_xVO_4$ by sol-gel method

were comparable to that of Lai et. al, (2002b) as presented in Figure 6.6 which shows increasing value of lattice constant with increasing of Mn content in the system.

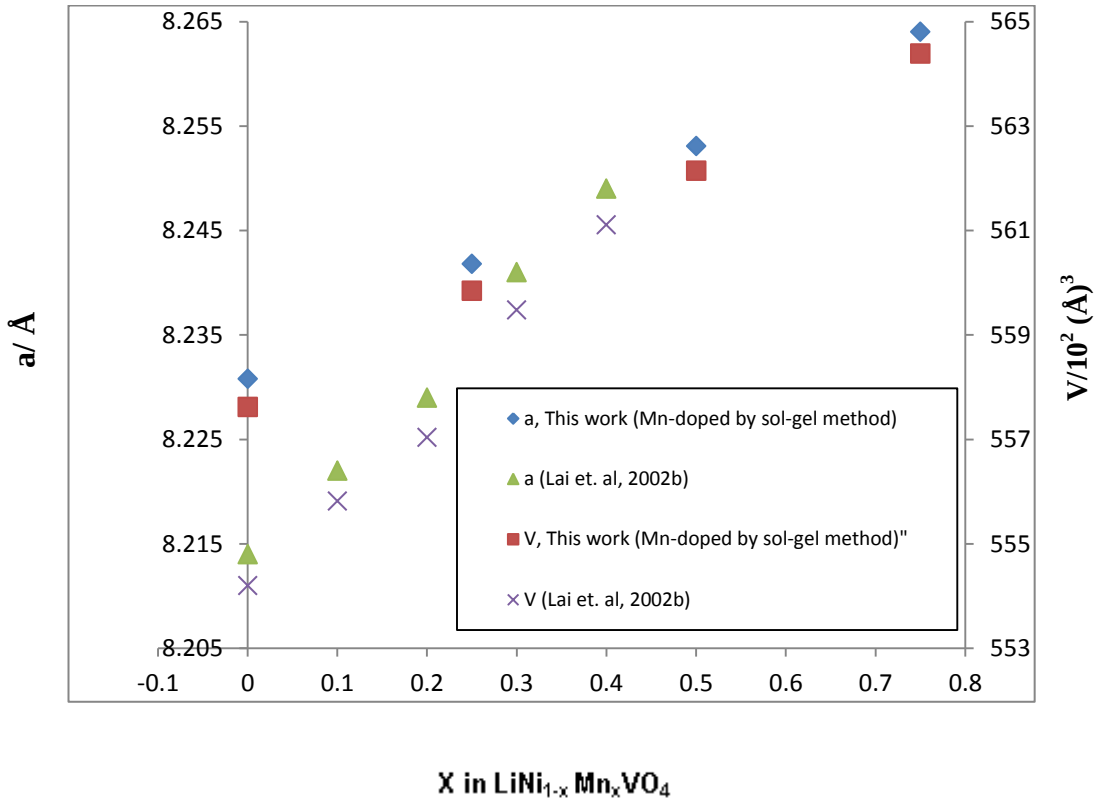

Figure 6.6 Lattice constants and the volumes of crystal cell for $LiNi_{1-x}Mn_xVO_4$ ($0 \leq x \leq 1$) by sol-gel method calcined at 600 °C.
For Lai et. al, (2002b) temperature is 750 °C

6.3 Chemical Reaction

The synthesis reaction of the $LiNi_{1-x}Mn_xVO_4$- SG system was suggested based on the observed reaction. Initially, the chemical reactions obtained in the mixed doped system are determined by considering the citric acid (complexing agent) poured into the solution. As a result, a clear dark purple solution was obtained for the mixed solution.

Thus, the V_2O_5 was formed as the acid reacted with the NH_4VO_3 [Tsaramyrsi *et. al*, 2001]. Here, the reaction of the mixing solution can be written as:

$$2NH_4VO_3 + 2C_6H_8O_7 \longrightarrow V_2O_5 + 2\,(NH_4)\,C_6H_7O_7 + H_2O \quad (6.1)$$

The mixing solution will then result in the formation of vigorous gas evolution in the synthesis. This phenomenon occur when the $LiCH_3COO{\cdot}2H_2O$, Ni $(CH_3COO)_2{\cdot}4H_2O$ and Mn $(CH_3COO)_2{\cdot}4H_2O$ reacted with citric acid, $C_6H_8O_7$. Thus, the CO_2 gas and $LiNi_{1-x}Mn_xC_6H_5O_7$ were produced:

$$LiCH_3COO{\cdot}2H_2O + 0.75\ Ni\ (CH_3COO)_2{\cdot}4H_2O + 0.25Mn(CH_3COO)_2{\cdot}4H_2O + C_6H_8O_7 + 6\ O_2 \longrightarrow LiNi_{0.75}Mn_{0.25}C_6H_5O_7 + 6CO_2 + 12H_2O \quad (6.2)$$

As reported by Tsaramyrsi, the V_2O_5 is an oxidant in an acidic solution [Tsaramyrsi *et. al*, 2001]. Therefore, the V_2O_5 may react with the citric acid, $C_6H_8O_7$ to form acidic complexes. The oxidation number V(V) in V_2O_5 can be reduced to V(IV) as the $(VO)^{2+}$ ion forms with the gas evolution. Thus, the production of $(NH_4)(VO)\ C_6H_5O_7$ is achieved when the $(VO)^{2+}$ ion was reacted with the $(NH_4)\ C_6H_7O_7$.

$$V_2O_5 + C_6H_8O_7 + 2(NH_4)C_6H_7O_7 + 4O_2 \longrightarrow 2(NH_4)(VO)C_6H_5O_7 + 6CO_2 + 6H_2O \quad (6.3)$$

The correlative reactions for synthesizing the mixed doped system are concluded by combining the above reactions:

$NH_4VO_3 + 2C_6H_8O_7 + LiCH_3COO{\cdot}2H_2O + 0.75\ Ni(CH_3COO)_2{\cdot}4H_2O + 0.25Mn(CH_3COO)_2{\cdot}4H_2O + 23/4\ O_2 \longrightarrow LiNi_{0.75}Mn_{0.25}C_6H_5O_7 + (NH_4)(VO)\ C_6H_5O_7 + 27/2\ H_2O + 6CO_2$ (6.4)

The product proposed in the equation above may result in formation of $LiNi_{0.75}Mn_{0.25}C_6H_5O_7$ (VO) $(NH_4)\ C_6H_5O_7$, as shown below. As the continuous heating process take place, the total decomposition equation in air atmosphere from the product of the total equation (6.4) can be written as:

$4LiNi_{0.75}Mn_{0.25}C_6H_5O_7{\cdot}\ (VO)\ {\cdot}\ (NH_4)\ C_6H_5O_7 + 37O_2 \longrightarrow 4LiNi_{0.75}\ Mn_{0.25}VO_4 + 48CO_2 + 22H_2O + 4NH_3$ (6.5)

6.4 Thermogravimetric Analysis (TGA)

The synthesizing process has obtained the dried gel of the mixed doped system producing the loose powder compound. The yielding intermediate product which called precursor was thermally analysed upon temperature ranging from 25 °C to 750 °C. The curves of TGA and DTGA for the mixed doped precursor are presented in Figure 6.7.

The continuation of weight loss was observed in the temperature range from room temperature to 100 °C at about 3.07 %. This behavior corresponds to the excess water removal and lithium acetate decomposition. Comparing with the undoped systems with the mixed doped system, there are several endo/exothermic peaks that occurs in the decomposition process. There are three main endothermic peaks in temperature range from 80 °C to 600 °C located at 80 °C, 371 °C, and 573 °C. This may be the result due

to the citric acid and ammonium metavanadate decomposed in the temperature ranged from 100 °C to 200 °C while manganese acetate decomposed at above 300 °C.

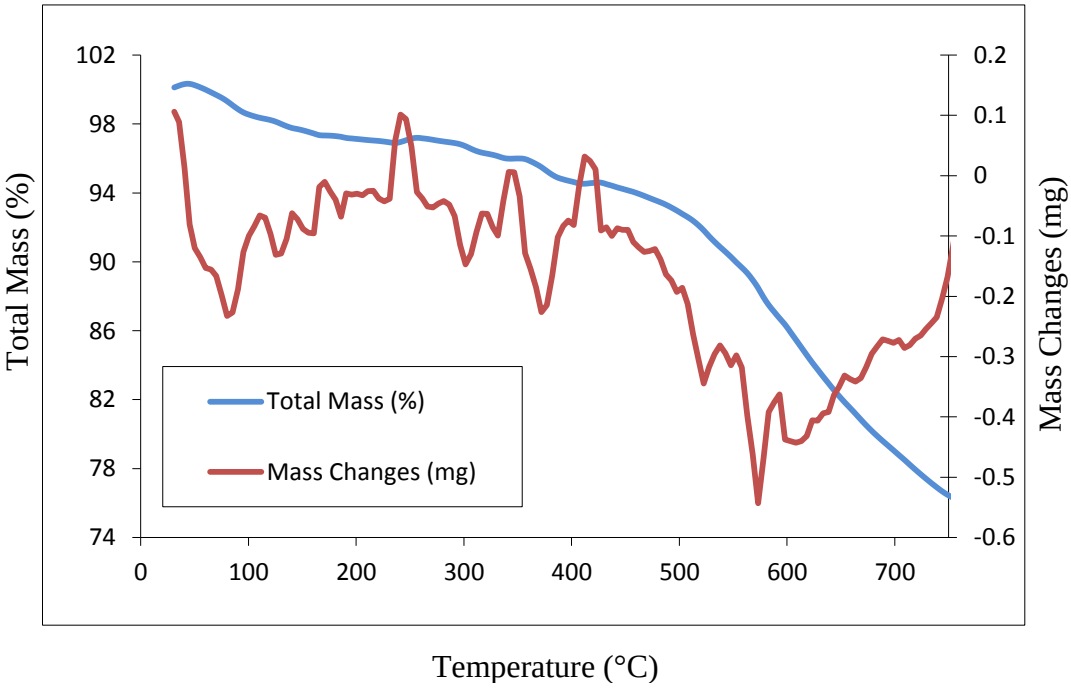

Figure 6.7 TGA and DTGA curve of the $LiNi_{1-x}Mn_xVO_4$- SG precursor

The exothermic peaks may due to the formation of the acid complexes as the result of acetates metal reacted with the citric acid. The additional of manganese acetate in the reaction mechanism might contribute in additional complexes decomposition process with the other intermediates. The aquired complexes along with the gas formation such as CO_2 and NH_3 may also promote the exothermic phenomenon that occur in the process. The decomposition process measured by the TGA study is 18.9 % of weight loss in the system.

6.5 Morphology studies

6.5.1 Scanning Electron Microscopy (SEM)

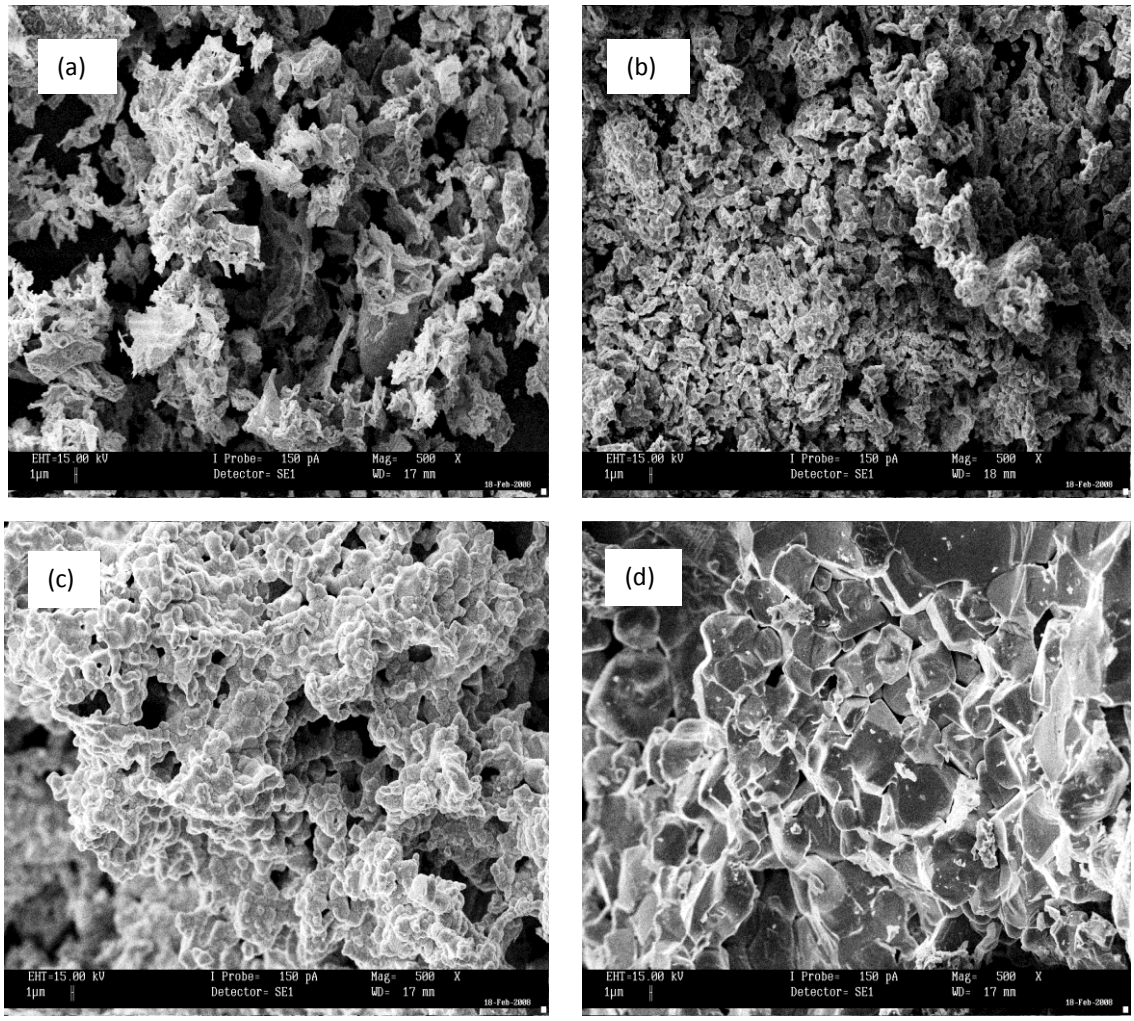

Figure 6.8: Surface morphology of $LiNi_{0.75}Mn_{0.25}VO_4$ – SG system at (a) 500 °C; (b) 600 °C; (c) 700 °C; (d) 800 °C with 500X magnification

Figure 6.8 shows the surface morphology for the $LiNi_{0.75}Mn_{0.25}VO_4$ – SG system. The system has been chosen for Mn = 0.25, the only compound in the system portray the pure phase of inverse spinel $LiNiVO_4$ by structural analysis in previous chapter. The doped compound was sintered at temperature range of 500 ºC - 800 ºC in a furnace. The SEM micrograph from Figure 6.8 (a to c) reveal the mixed doped compound in the system exhibit almost similar to obtained microstructure of both $LiNiVO_4$ synthesized by the sol-gel and polymer precursor method.

The samples have smaller voids and formation of growing spherical clustered particles upon higher sintering temperature. However, the particle shown in Figure 6.8 (d) displays polyhedral geometry and more densified microstructure. Additionally, the acquired image registers roughly isotropic particle structure. The obtained polyhedral particle can be compared with the work reported by Fey and Perng, (1997) and Lu and Liou, (1999) who as well gained polyhedral particle structure upon their synthesizing method.

6.5.2 Transmission Electron Microscope (TEM)

The TEM images of $LiNi_{0.75}Mn_{0.25}VO_4$ – SG system products are shown in Figure 6.8. It was clearly revealed that the particles had almost defined spherical shapes. The sticking particle clusters in Figure 6.9 (a and b) explain the same SEM images obtained at lower sintering temperature. The particle size in Figure 6.9 a (i) and Figure 6.9 a (ii) are 33.3 nm and 27.8 nm respectively. Agglomeration was exhibited as the heating temperature rose up as shown in Figure 6.9 (b). The particle sizes depicted in Figure 6.9 c (i), Figure 6.9 c (ii), Figure 6.9 c (iii) is 37.9 nm, 27.5 nm and 24.1 nm, respectively. The particle shapes are also has well defined crystal structure. The doped $LiNi_{0.75}Mn_{0.25}VO_4$ – SG crystalline also pictures spherical nanoparticles with obviously narrower in size distribution. The particle of the compound crystallized at size nearly~ 30.0 nm. Figure 6.9 d (i) shows crystal size of 20.0 nm while in Figure 6.9 d (ii) the crystal size is 32.0 nm. The particle size in Figure 6.9 d (iii) is 24.0 nm. This result suggests that the addition of manganese has led to the shrinkage of particle size at highest heating temperature at 800 °C for better dispersivity. Thus, the particle size distribution may contribute/improve better kinetics during intercalation/deintercalation process [Subramania *et. al*, 2006].

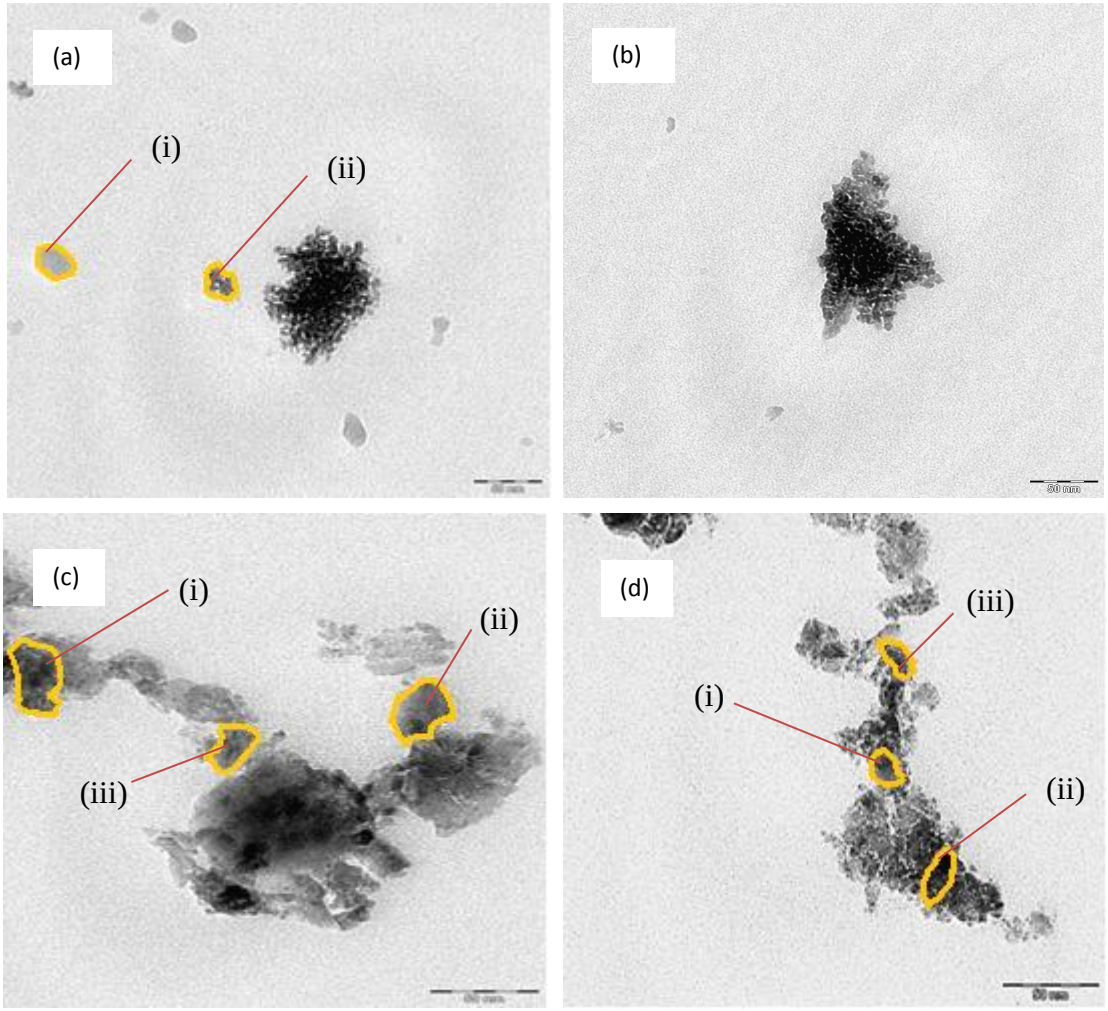

Figure 6.9: TEM images of $LiNi_{0.75}Mn_{0.25}VO_4$ – SG system at (a) 500 °C; (b) 600 °C; (c) 700 °C; (d) 800 °C

6.6 Elemental Studies (EDAX)

The EDAX data for mixed doped vanadate, $LiNi_{0.75}Mn_{0.25}VO_4$ is tabulated in Table 6.3. The results shown in Figure 6.10 gave the average atomic percentage of Ni: Mn upon all heating temperatures. The Mn doping element in the compound was also detected in the analysis. The Ni: Mn ratio was having very close value to 0.75: 0.25. Thus, the compound can be said in accordance with the stoichiometric composition of

$LiNi_{0.75}Mn_{0.25}VO_4$ chemical formulae. The obtained data also indicated that the Ni^{2+} and Mn^{2+} ions did not change during the synthesis and even after sintering process.

Table 6.3: Atomic ratio (%) of Ni and Mn for inverse spinel $LiNi_{0.75}Mn_{0.25}VO_4$ on various sintering temperatures.

Temperature (°C)	Ni	Mn	Ni : V
500 °C	25.42	5.11	4.9746 : 1
600 °C	11.94	4.23	2.8227 : 1
700 °C	11.57	4.35	2.6598 : 1
800 °C	16.14	7.40	2.1810 : 1

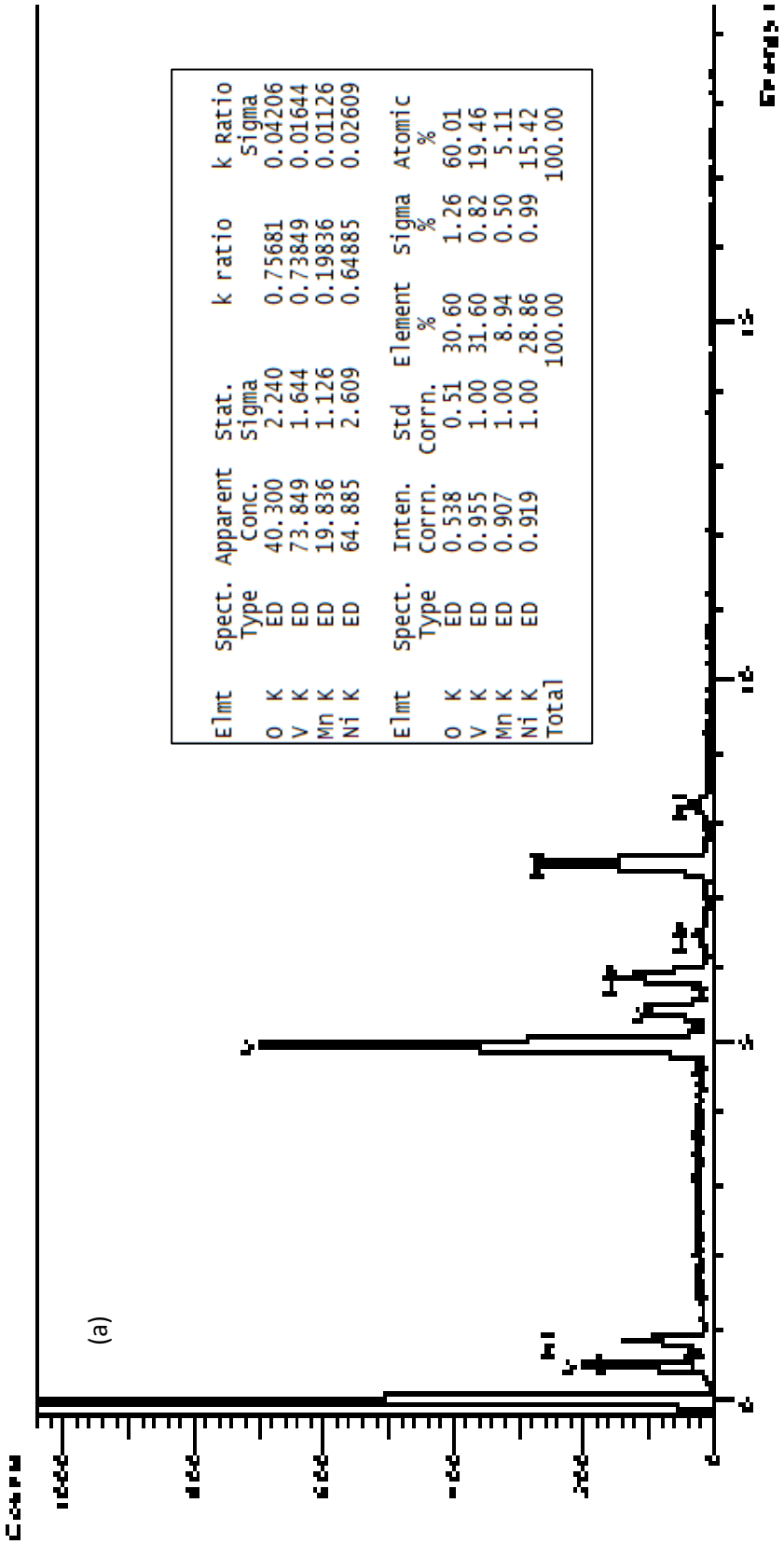

Figure 6.10 (a): EDAX analysis of the $LiNi_{0.75}Mn_{0.25}VO_4$ at 500 °C

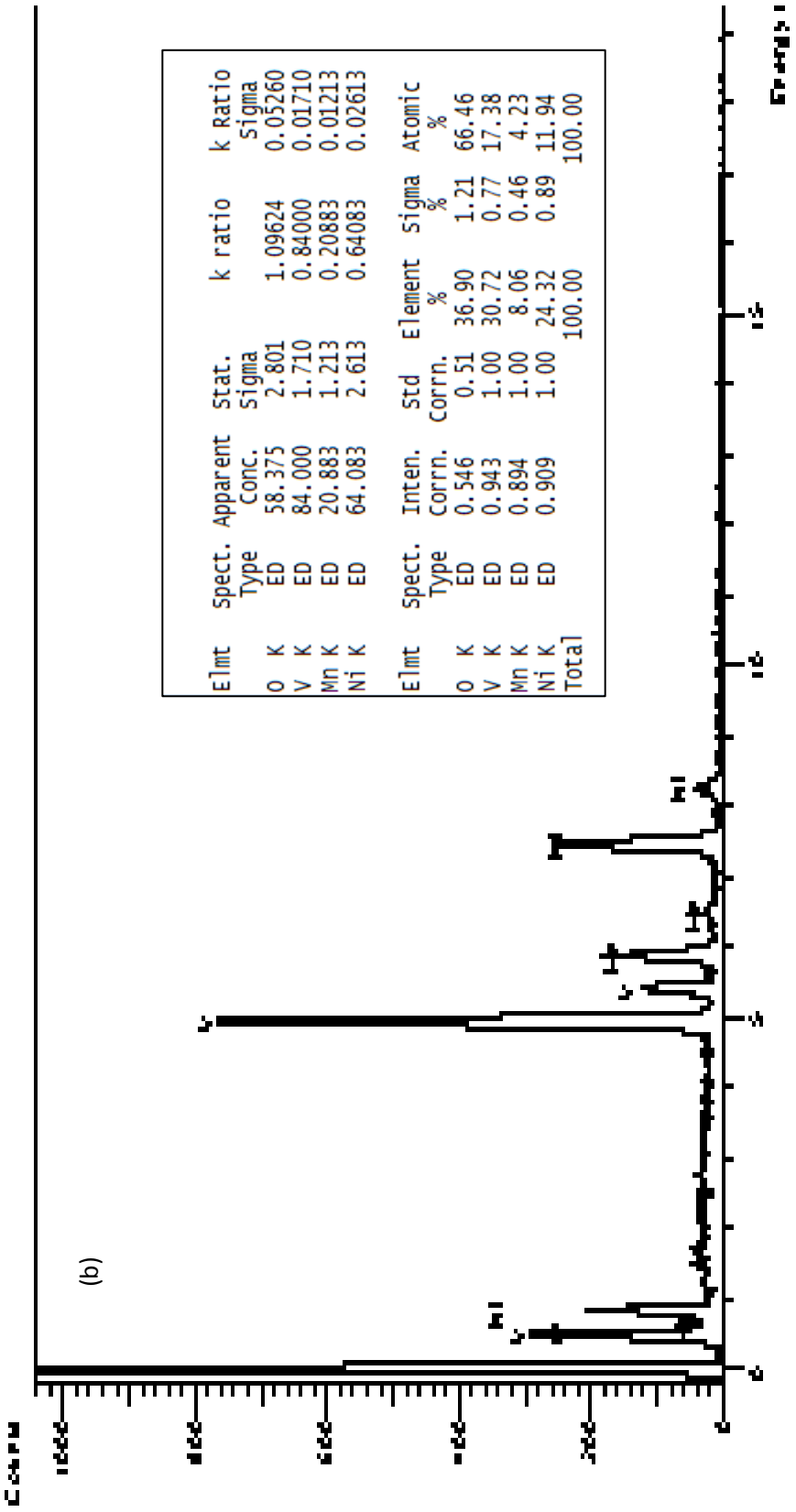

Figure 6.10 (b): EDAX analysis of the $LiNi_{0.75}Mn_{0.25}VO_4$ at 600 °C

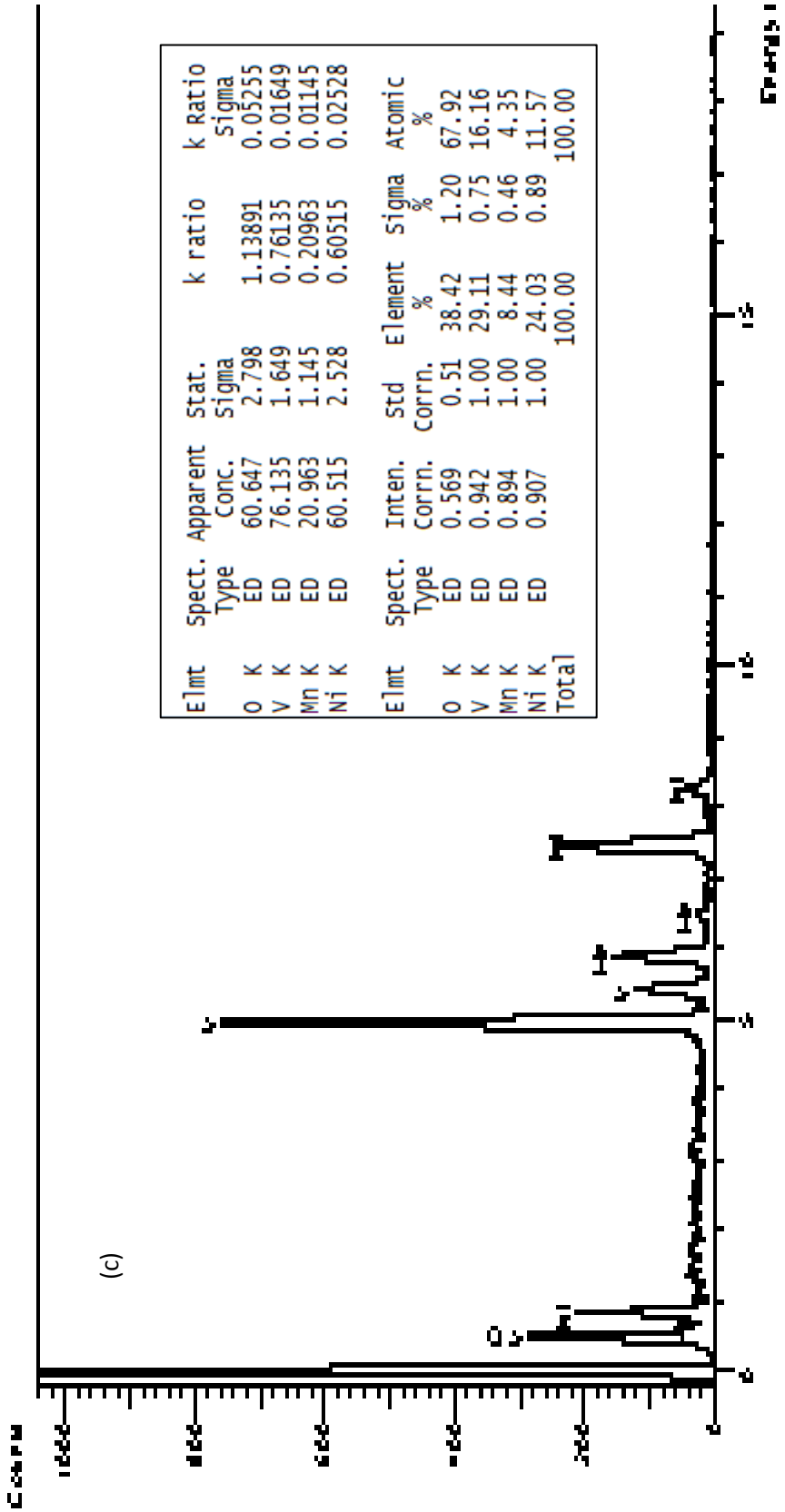

Figure 6.10 (c): EDAX analysis of the $LiNi_{0.75}Mn_{0.25}VO_4$ at 700 °C

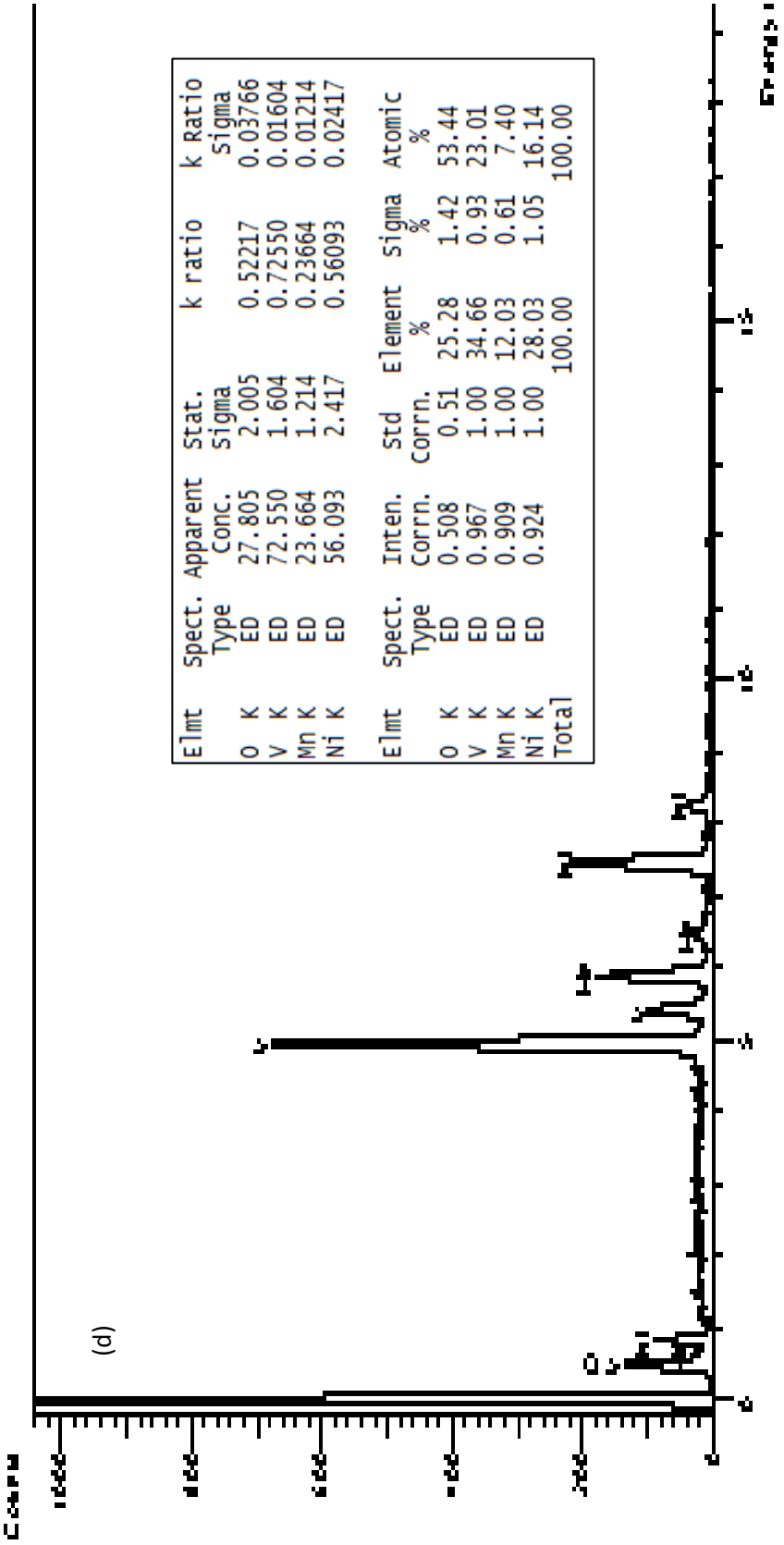

Figure 6.10 (d): EDAX analysis of the $LiNi_{0.75}Mn_{0.25}VO_4$ at 800 °C

6.7 Cyclic voltammetry (CV)

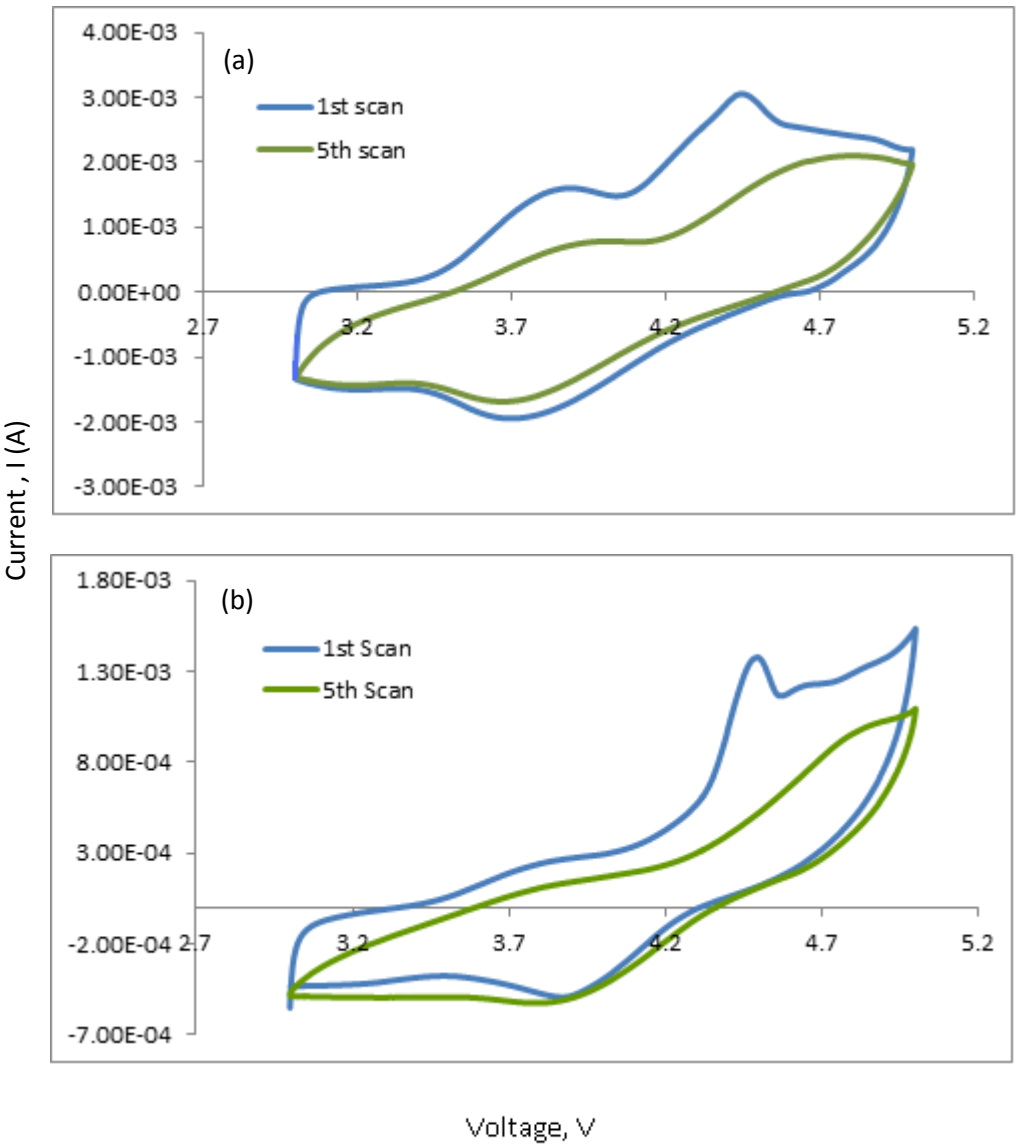

Figure 6.11: Cyclic voltammograms for Li/ $LiNi_{0.75}Mn_{0.25}VO_4$ – SG electrode system in 1 mol dm^{-1} $LiPF_6$ in 1:2 by (vol/ vol%) EC/DMC at scan rate of 1 mV/s (a) cathode sintered at 500 °C; (b) cathode sintered at 800 °C

Figure 6.11 represents the cyclic voltammogram (CV) curves for Li/ $LiNi_{0.75}Mn_{0.25}VO_4$ – SG measured at room temperature. The fabricated cell was recorded at 1 mV/s of scan rate between 3-5 V. The CV curve demonstrates oxidation and reduction peaks which correspond to the single electron transfer process in Li- de/ intercalation process. The

voltammogram reveal the reversible nature of the doped cathode system. The CV curves displays the typical characteristic redox behavior having prominent peak at anodic process. The redox mechanism remains almost unchanged upon cycling which implies the reversibility of the electrochemical process. The voltammogram features CV curve upon different annealing temperature for the prepared cathode system. The measurement of the cyclic voltammetry in Figure 6.11 (a) for the doped $LiNi_{0.75}Mn_{0.25}VO_4$ sintered at the 500 °C show an obvious oxidation peak that was not clearly observed in the undoped system during the 1st scan. The appearance of the peak of the oxidation curve at 4.3 V was observed. The potential separation on the anodic scan is 0.6 V at the initial scan. The reduction peak was noticed at 3.7 V at the initial scan. However, the area under curve for the system was reduced suggesting the capacity fading upon cycling after a few scans. The redox curves in Figure 6.11 (b) were obviously decreasing for the coated active material at 800 °C. The anodic peak was clearly observed at 4.4 V during initial scan. This behavior demonstrates 0.7 V of potential separation. On the other hand, the curve area of the voltammogram decline dramatically with increasing cycle number in the 5th cycle. This behavior suggests the structural degradation of the inverse spinel structure electrode.

6.8 Summary

The mixed- doped $LiNi_{0.75}Mn_{0.25}VO_4$ have been successfully prepared by the sol- gel method. The XRD diffractogram show the similar behavior of cubic crystal inverse spinel $LiNiVO_4$. This method also allows the formation of the single phase of the structure without any impurities. The reaction mechanism was also proposed in this work and only a small total weight loss (18.9 %) of the precursor was observed by the thermal analysis study.

The crystallite size obtained from the calculation through Scherer equation has shown that the crystal size decreases upon higher sintering temperature. These results were confirmed with the TEM images that correspond to the calculated crystallite size obtained by the FWHM from XRD data analysis. The size ranging from 35.71 nm to 23.65 nm was obtained for the $LiNi_{0.75}Mn_{0.25}VO_4$ system. The EDAX measurement for the mixed doped system in this work was stoichiometrically agrees with the vanadate proportional formula.

The voltammogram of the system represent noticeable oxidation/ reduction peak at initial scans which display the nature of the redox behaviour for the cell in the system. However the presence of the peak was no longer appearing after the 1^{st} scan onwards. The redox curve area decreases for the active material sintered at 800 °C and show capacity decline upon few cycles. Based on the voltage difference during initial scan and the area of redox peaks during cycling, the cathode sintered at lower temperature gives better reversibility on the de/intercalation process.